

EFFECT OF THE MODIFIER ION ON THE PROPERTIES OF MgFe₂O₄ AND ZnFe₂O₄ PIGMENTS

Camila S. Xavier^{1*}, R. A. Candeia¹, M. I. B. Bernardi², S. J. G. Lima³, E. Longo⁴,
C. A. Paskocimas⁵, L. E. B. Soledade¹, A. G. Souza¹ and Iêda M. G. Santos¹

¹LTM, Departamento de Química/CCEN, Universidade Federal da Paraíba, Campus I, CEP 58059-900, João Pessoa, PB, Brazil

²CMDMC, Instituto de Física de São Carlos, USP, São Carlos, SP, Brazil

³LSR, Departamento de Engenharia Mecânica/CT, Universidade Federal da Paraíba, Campus I, João Pessoa, PB, Brazil

⁴CMDMC-LIEC, Instituto de Química, UNESP, Araraquara, SP, Brazil

⁵DM/CT, Universidade Federal do Rio Grande do Norte, Natal, RN

Magnesium and zinc ferrites have been prepared by the polymeric precursor method. The organic material decomposition was studied by thermogravimetry (TG) and differential thermal analysis (DTA). The variation of crystalline phases and particle morphology with calcination temperature were investigated using X-ray diffraction (XRD) and scanning electronic microscopy (SEM), respectively. The colors of the ferrites were evaluated using colorimetry. Magnesium ferrite crystallizes above 800°C, presenting a yellow-orange color with a reflectance peak at the 600–650 nm range, while zinc ferrite crystallizes at 600°C, with a reflectance peak between 650–700 nm, corresponding to the red-brick color.

Keywords: magnesium ferrite, Pechini, thermal analysis, zinc ferrite

Introduction

Mixed oxides with spinel structure have several applications. They are known as pigments with high thermal chemical stability, thus suitable for coloring enamels and ceramics [1]. Some spinel type compounds are also excellent refractory [2], magnetic [3] and catalytic materials [4, 5].

The spinel structure is made up by a face-centered cubic close-packed oxygen sublattice in which a fraction of the tetrahedral (T) and octahedral (O) sites are filled [6]. The crystal structure of spinel ferrites can be formulated in greater detail as $(M_{1-\lambda}Fe_\lambda)[M_xFe_{2-\lambda}]O_4$. The parentheses and the square brackets denote cation sites of fourfold (T) and sixfold [O] oxygen coordination, respectively [7]. λ represents the so-called degree of inversion (defined either as the fraction of the (T) sites occupied by Fe³⁺ cations or as the fraction of the [O] sites occupied by M²⁺ cations. It is widely appreciated that the cation distribution in spinel ferrites, upon which many physical and chemical properties depend [8], is a complex function of processing parameters.

Magnesium ferrite, MgFe₂O₄, is a soft magnetic *n*-type semiconducting material [9], which finds a number of applications in heterogeneous catalysis, adsorption, sensors, and in magnetic technologies. The structural formula of magnesium ferrite is usually written as (Mg_{1-x}Fe_x)[Mg_xFe_{2-x}]O₄ [10].

The structural formula of zinc ferrite is usually written as (Zn_{1-δ}²⁺Fe_δ³⁺)(Zn_δ²⁺Fe_{2-δ}³⁺)O₄²⁻. There are two

ordered configurations stable at low temperature, the one with $\delta=0$ (normal spinel) and the other with $\delta=1$ (inverse spinel) [6].

Different techniques have been reported for the synthesis of ferrites. The ceramic method [11–13], in which the components are thoroughly mixed and calcined at high temperatures, is the most common one, but the high temperatures involved lead to grain growth. Other methods that have been reported are high-energy ball milling [11], sol-gel [14], co-precipitation from salts followed by calcinations at high temperatures [15–18] and hydrothermal routes [19–22]. Recently, the liquid mix process (the so-called polymeric precursor method) has also been successfully used for the preparation of ferrites [23]. In this process, an intermediate precursor of metallic salt and iron is formed using citric acid and ethylene glycol, which, on calcination, breaks down to yield the ferrite [24].

In the present investigation, we synthesized magnesium or zinc ferrites by the polymeric precursor method, in order to evaluate the effect of the divalent cation (the modifier ion) on the structural, morphological and optical properties of the ferrites.

Experimental

Ferrites were synthesized by the polymeric precursor method. More details of the preparation method can be

* Author for correspondence: camilasxavier@yahoo.com.br

found in [25]. The starting materials were citric acid (Vetec, 99.5% purity), iron nitrate (Vetec, 98.0% purity) and magnesium carbonate (Aldrich, 99.0% purity) or zinc acetate (Vetec, >98.0% purity). A stoichiometric proportion of 3:1 citric acid:metal molar ratio was used. For citric acid:ethylene glycol (Vetec, 99.5% purity), a mass proportion of 60:40 was used.

The thermal decomposition of the powder precursors was studied by thermogravimetry and differential thermal analysis using TA Instruments, SDT-2960. About 10 mg of the material were weighed in alumina crucibles and heated at $10^{\circ}\text{C min}^{-1}$ up to 1000°C under air atmosphere at a flow rate of 50 mL min^{-1} .

After heat treatment between 600 and 1000°C , the pigment was obtained. The evaluation of the crystalline phases and the determination of the lattice parameters were carried out by X-ray diffraction (XRD), using SiO_2 as an external standard. The measurements were obtained using a D-5000-Siemens diffractometer with CuK_{α} radiation, at room temperature.

Scanning electronic microscopy (SEM) was used to characterize the morphology of the pigments using a 1430-LEO equipment.

The L^* , a^* and b^* color parameters of samples were measured using the Gretag Macbeth Color-eye spectrophotometer 2180/2180 UV, in the 360 – 750 nm range, using the D65 illumination. The CIE- $L^*a^*b^*$ colorimetric method, recommended by the CIE (Commission Internationale de l'Eclairage) was followed. In this method, L^* is the lightness axis [black (0) white (100)], b^* is the blue (–) yellow (+) axis and a^* is the green (–) red (+) axis [26].

Results and discussion

TG/DTA curves of the MgFe_2O_4 and ZnFe_2O_4 precursors are illustrated in Fig. 1 and Table 1. For the MgFe_2O_4 precursors, two decomposition steps were observed. The first peak about 100°C , is related to the loss of water and some gases adsorbed on the surface. The second peak about 461°C is due to the decomposition of the organic matter. For ZnFe_2O_4 four decomposition steps were observed, the first peak about 78°C is also related to the loss of water and some gases adsorbed on the surface and the remaining three peaks (339 , 425 and 489°C) are due to the decomposition of

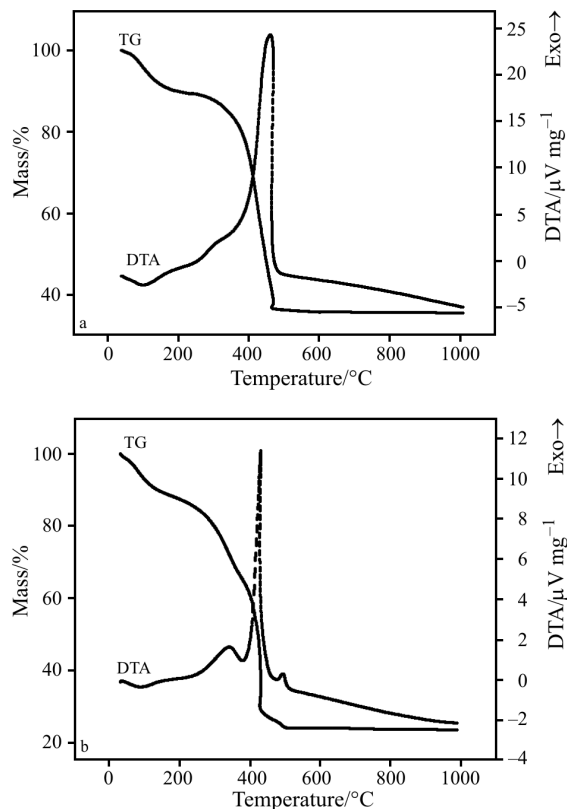


Fig. 1 TG/DTA curves of the powder precursors calcined at 300°C for 1 h; a – MgFe_2O_4 and b – ZnFe_2O_4

the organic matter. For both precursors, the DTA curves showed sharp exothermic peaks, due to the combustion reaction of the organic matter. Considerable mass loss corresponds to the combustion of the organic material, which began at around 221°C for the magnesium ferrite and at 150°C for the zinc ferrite and finished below 500°C for both ferrites [24].

XRD patterns are presented in Figs 2a and b, for MgFe_2O_4 and ZnFe_2O_4 , respectively. MgFe_2O_4 crystallization starts at about 600°C , but a high crystalline material is only observed above 800°C . On the other hand, ZnFe_2O_4 presents a high crystallinity even a temperature as low as 600°C . Both materials did not present intermediate phases. At 1000°C , the peaks are well defined, as a consequence of the organization of the material structure.

It may be observed that crystallization does not depend only on the elimination of the organic material. The two ferrites are thermally stable above 500°C , as indicated by TG, but the crystallization process is quite different, due to the properties of the modifiers. In the present case, magnesium leads to more covalent bonds than zinc. As covalent bonds are more directional than the ionic bonds, the crystalline structure presents a higher distortion, being more difficult to crystallize.

Table 1 Data taken from TG and DTA curves

Sample	Step	$T_i/{}^{\circ}\text{C}$	$T_p/{}^{\circ}\text{C}$	$T_f/{}^{\circ}\text{C}$	$\Delta m/\%$
MgFe_2O_4	1 st	40	100 (endo)	237	10.5
	2 nd	237	461 (exo)	471	53.8
ZnFe_2O_4	1 st	44	78 (endo)	158	9.8
	2 nd	158	339 (exo)	373	23.2
	3 rd	373	425 (exo)	460	39.2
	4 th	460	489 (exo)	507	2.4

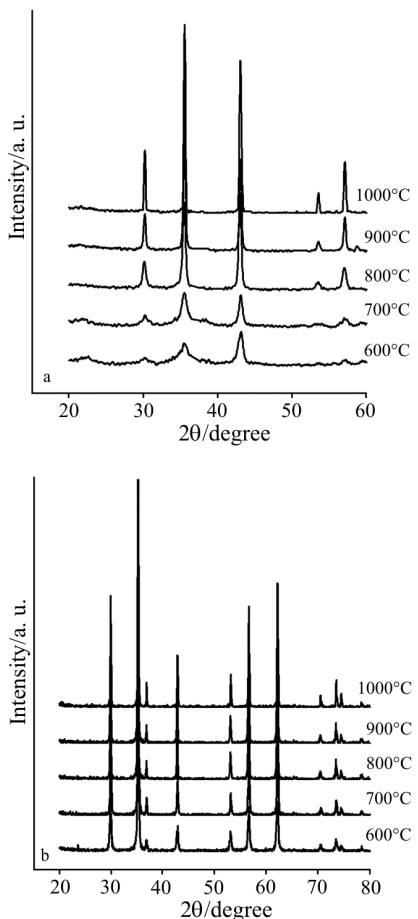


Fig. 2 XRD patterns of the materials as a function of the heat treatment temperature; a – MgFe₂O₄ and b – ZnFe₂O₄

Using XRD results, the crystallite sizes were calculated, as presented in Fig. 3. The organization of the material is a thermally activated process, as indicated by the crystallite size increase with temperature. It may also be observed that the crystallites of zinc ferrite are bigger than the ones of magnesium ferrite. This is also related to the covalent character of magnesium, what makes crystallization more difficult, leading to smaller crystallites.

The lattice parameter values are presented in Fig. 4. The theoretical data were obtained in JCPDS cards 36-0298 and 22-1012 for MgFe₂O₄ and ZnFe₂O₄, respectively. The small lattice parameter value of MgFe₂O₄ at 600°C is probably due to the low crystallinity of this material, with high amount of defects, as indicated by the XRD pattern and FWHM value. For ZnFe₂O₄, a high crystallinity is observed at 600°C, leading to a lattice parameter similar to its theoretical figure. Both ferrites presented this similarity at 700 and 800°C, indicating that the materials have already a high crystallinity. A decrease in the lattice parameter values is observed at 900°C, for both materials. According to the literature, this behavior may be related to order-disorder phase transitions or to nor-

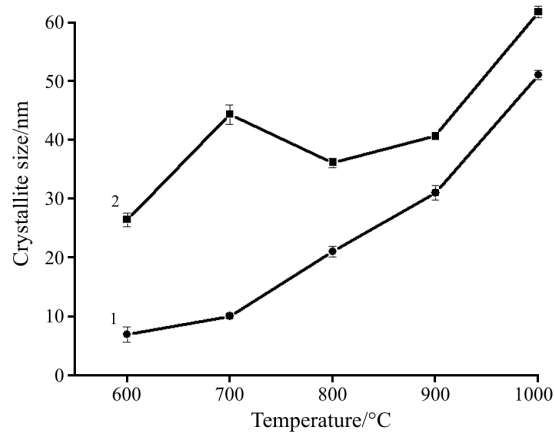


Fig. 3 Crystallite size as a function of the heat treatment temperature, for 1 – MgFe₂O₄ and 2 – ZnFe₂O₄ powders

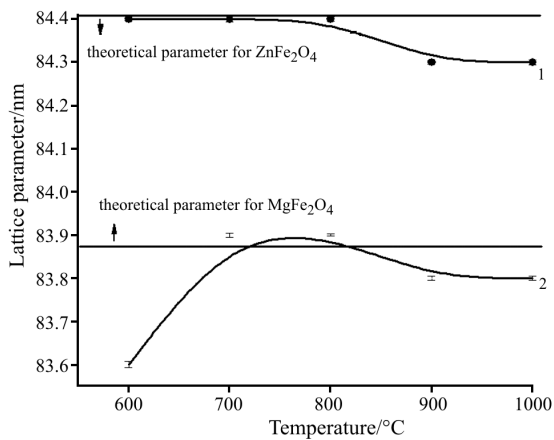


Fig. 4 Lattice parameter as a function of the heat treatment temperature, for 1 – MgFe₂O₄ and 2 – ZnFe₂O₄ powders

mal-inverse spinel transitions, as a consequence of temperature increase [27–29].

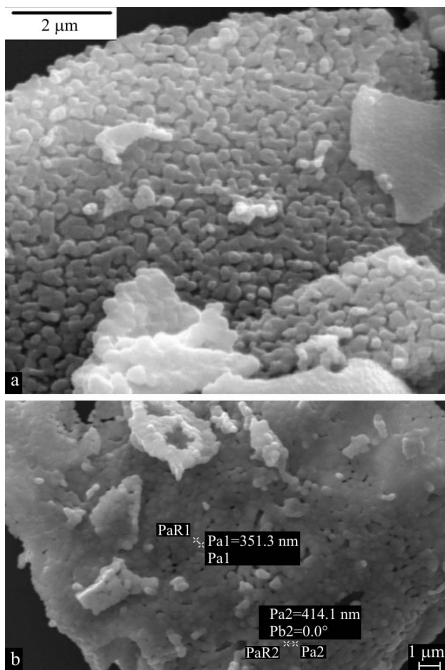
The morphologies of the powders are presented in Fig. 5. At 1000°C, both materials are highly sintered with the presence of aggregates, indicated by the neck formation.

A higher diffusion rate occurs in ZnFe₂O₄ samples, indicated by the lower porosity of the aggregate as a consequence of the particle coalescence process. This result agrees with the crystallite sizes observed (Fig. 3).

The reflectance curves of the MgFe₂O₄ and ZnFe₂O₄ samples in the visible region are presented in Fig. 6. For MgFe₂O₄, a continuous increase in reflectance is observed up to 700 nm, leading to a yellow-orange color with a high stability up to 750°C. For ZnFe₂O₄, the maximum reflectance occurs between 650–700 nm, leading to a red-brick color with a high stability up to 600°C. Both temperatures of stability of the color are evidenced by evolution of the crystalline phases indicated on XRD patterns. According to Sepelák, magnesium ferrite is an intermediate spinel, with both cations occupying tetrahedral and octahedral

Table 2 Colorimetric coordinates of ferrites calcined at different temperatures

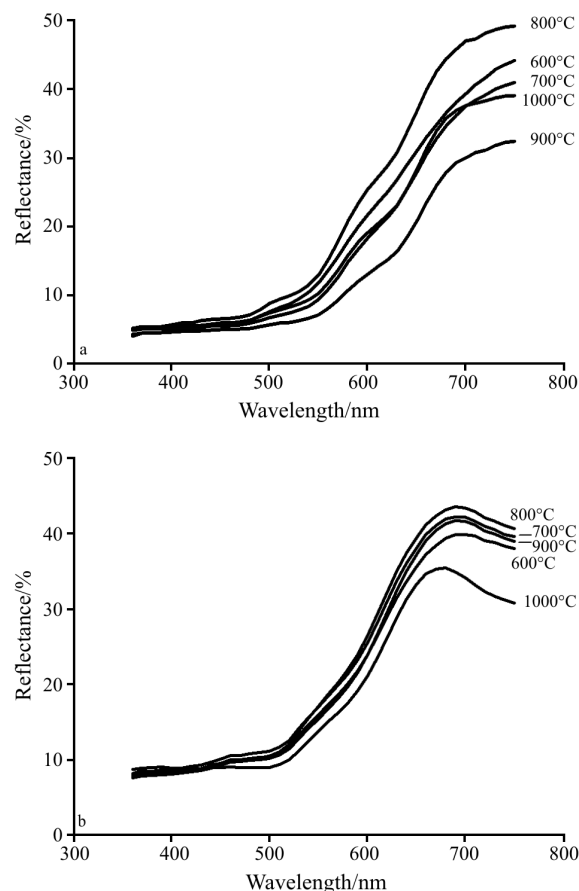
Temperature/°C	MgFe ₂ O ₄			ZnFe ₂ O ₄		
	a*	b*	L*	a*	b*	L*
600	21.36	31.53	47.67	16.73	18.32	43.36
700	21.62	26.57	44.09	17.17	19.89	42.63
800	23.37	33.16	50.69	15.84	16.32	40.59
900	18.21	19.84	38.39	13.50	12.34	38.56
1000	20.26	26.74	45.19	15.04	11.67	37.34

**Fig. 5** SEM of the ferrites heat treated at 1000°C; a – MgFe₂O₄ and b – ZnFe₂O₄

sites [10]. On the other hand, zinc ferrite, is a normal spinel, with zinc in tetrahedral and iron in the octahedral sites [6]. So, when zinc is used as modifier, Fe³⁺ presents only one coordination (6-fold), with one type of splitting of the d orbitals. When Mg²⁺ is used, two coordination types are observed for Fe³⁺ (6-fold and 4-fold), with two types of splittings. Therefore, more absorption regions are present in MgFe₂O₄, with a more defined reflectance region. On the other hand, different synthesis procedures may lead to different colors due to a change in the degree of inversion.

The colorimetric coordinates (Table 2) vary according to the heat treatment temperature and to the modifier cation. A randomic behavior is observed in relation to temperature, probably due to crystallization associated to phase transitions, changing the ligand field around the chromophore ion (iron).

In relation to the modifier cation, Mg²⁺ is more covalent than Zn²⁺ with more directional bonds. The higher covalence increases the distortion of the unit cell, leading to the Jahn–Teller effect, with a new splitting of the e_g and t_{2g} orbitals. As a consequence, new

**Fig. 6** Reflectance spectra in the visible region of ferrites heat treated at different temperatures; a – MgFe₂O₄ and b – ZnFe₂O₄

energy levels are created within the band gap, causing electron transitions with smaller energy and higher wavelength. Hence, magnesium ferrite presents higher a* and b* values, with more intense colors.

Conclusions

Magnesium and zinc ferrites were successfully obtained using the polymeric precursor method. In spite of the lower final temperature of mass loss, observed in magnesium ferrite, a high crystallinity material is only observed at around 750°C. For zinc ferrite, a high crystallinity is already observed at 650°C.

The higher covalent character of the magnesium–oxygen bond leads to a lower long range periodicity, increasing the crystallization temperature. As a consequence a lower diffusion is observed, with smaller crystallite size and a less sintered aggregated.

Different colors were obtained according to the modifier ion and to the calcination temperature. In relation to colors, the deformation of unit cell leads to the Jahn–Teller effect, increasing the possible electronic transitions in visible region, forming more intense colors.

Acknowledgements

The authors acknowledge the financial support of the Capes, CNPq/MCT and FAPESQ.

References

- 1 W. Büchner, R. Schliebs, G. Winter and K. H. Büchel, *Industrial Inorganic Chemistry*, VCH Verlagsgesellschaft, Weinheim 1989, p. 543.
- 2 A. R. West, *Solid State Chemistry and Its Applications*, John Wiley & Sons, Chichester 1984, p. 569.
- 3 W. Büchner, R. Schliebs, G. Winter and K. H. Büchel, *Industrial Inorganic Chemistry*, VCH Verlagsgesellschaft, Weinheim 1989, p. 432.
- 4 G. Delpiero, F. Trifiro and A. Vacari, *J. Chem. Soc. Chem. Commun.*, 10 (1984) 656.
- 5 Z. Kowalczyk and S. Jodzis, *Appl. Catal.*, 58 (1990) 29.
- 6 S. Bid and S. K. Pradhan, *Mater. Chem. Phys.*, 82 (2003) 27.
- 7 K. E. Sickafus, J. M. Wills and N. W. Grimes, *J. Am. Ceram. Soc.*, 82 (1999) 3279.
- 8 M. A. Willard, Y. Nakamura, D. E. Laughlin and M. E. McHenry, *J. Am. Ceram. Soc.*, 82 (1999) 3342.
- 9 R. J. Willey, P. Noirclerc and G. Busca, *Chem. Eng. Commun.*, 123 (1993) 1.
- 10 V. Sepelák, D. Schultze, F. Krumeich, U. Steinike and K. D. Becker, *Solid State Ionics*, 141–142 (2001) 667.
- 11 C. N. Chinnasamy, A. Narayanasamy, N. Ponpandian, K. Chattopadhyay, H. Guérault and J. M. Grenache, *Scripta Mater.*, 44 (2001) 1407.
- 12 C. N. Chinnasamy, A. Narayanasamy, N. Ponpandian and K. Chattopadhyay, *Mat. Sci. Eng. A*, 304–306 (2001) 983.
- 13 W. Schiessl, W. Potzel, H. Karzel, M. Steiner, G. M. Kalvius, A. Martin, M. K. Krause, I. Halevy, J. Gal, W. Schäfer, G. Will, M. Hillberg and R. Wappling, *Phys. Rev. B*, 53 (1996) 9143.
- 14 A. S. Albuquerque, J. D. Ardisson, A. A. Waldemar and A. Macedo, *J. Magn. Magn. Mater.*, 192 (1999) 277.
- 15 T. Sato, K. Haneda, M. Seki and T. Iijima, *Appl. Phys. A*, 50 (1990) 13.
- 16 M. R. Anantharaman, S. Jagatheesan, K. A. Malini, S. Sindhu, A. Narayanasamy, C. N. Chinnasamy, J. P. Jacobs, S. Reijne, K. Seshan, R. H. H. Smits and H. H. Brongersma, *J. Magn. Magn. Mater.*, 189 (1998) 83.
- 17 M. Yokoyama, E. Ohta, T. Sato and T. Sato, *J. Magn. Magn. Mater.*, 183 (1998) 173.
- 18 T. Kamiyama, K. Haneda, T. Sato, S. Ikeda and H. Asano, *Solid State Commun.*, 81 (1992) 563.
- 19 C. Rath, K. K. Sahu, S. Anand, S. K. Date, N. C. Mishra and R. P. Das, *J. Magn. Magn. Mater.*, 202 (1999) 77.
- 20 C. Rath, N. C. Mishra, S. Anand, R. P. Das, K. K. Sahu, C. Upadhyay and H. C. Verma, *Appl. Phys. Lett.*, 76 (2000) 475.
- 21 C. Upadhyay, H. C. Verma, C. Rath, K. K. Sahu, S. Anand, R. P. Das and N. C. Mishra, *J. Alloys Compd.*, 326 (2001) 94.
- 22 J. L. Martín de Vidales, A. López-Delgado, E. Vila and F. A. López, *J. Alloys Compd.*, 287 (1999) 276.
- 23 F. J. Guaita, H. Beltran, E. Cordoncillo, J. B. Carda and P. Escribano, *J. Eur. Ceram. Soc.*, 19 (1999) 363.
- 24 A. Kundu, S. Anand and H. C. Verma, *Powder Technol.*, 132 (2003) 131.
- 25 R. A. Candeia, M. A. F. Souza, M. I. B. Bernardi, S. C. Maestrelli, I. M. G. Santos, E. Longo and A. G. Souza, *Mater. Res. Bull.*, 41 (2006) 183.
- 26 J. D. Cunha, D. M. A. Melo, A. E. Martinelli, M. A. F. Melo, I. Maia and S. D. Cunha, *Dyes Pigments*, 65 (2005) 12.
- 27 S. M. Yunus, H. S. Shimb, C. H. Leeb, M. A. Asgarc, F. U. Ahmeda and A. K. M. Zakariaa, *J. Magn. Magn. Mater.*, 232 (2001) 121.
- 28 J. Darul, W. Nowicki, P. Piszora, C. Baehtz and E. Wolska, *J. Alloys Compd.*, 401 (2005) 60.
- 29 M. Vucinic-Vasic, J. Blanusa, S. Rakic, A. Kremenovic, A. S. Nikolic and A. Kapor, *Appl. Phys. A*, 82 (2006) 49.

DOI: 10.1007/s10973-006-7744-6